LCLS-II Cu Linac KPP Results

Heinz-Dieter Nuhn[a]

[a]SLAC National Accelerator Laboratory, Stanford University, CA 94309-0210, USA

ABSTRACT

The LCLS-II project at SLAC successfully went through the first commissioning phases, i.e. the commissioning of the operation of the new undulator and dump lines with electrons from the Cu linac. The facility has been providing regular user beam since the Fall of 2020. This document examines how the Key Performance Parameters (KPPs) for this part of the project have been met.

Keywords: commissioning, x-ray FEL, LCLS-II

1. INTRODUCTION

SLAC has previously successfully developed, constructed and commissioned the world's first x-ray **F**ree **E**lectron **L**aser (FEL), funded, as the LCLS construction project, by the U.S. Department of Energy, Basic Energy Sciences (USDOE), with first lasing in April 2009. In 2013, USDOE started funding the LCLS-II upgrade project, which is now close to completion. It includes replacing the original LCLS undulator line by two new undulator lines: (1) one to produce vertically polarized x-ray pulses in the hard x-ray (HXR) wavelengths range and (2) another one to produce horizontally polarized x-ray pulses in the soft x-ray (SXR) wavelengths range. The project also includes a new superconducting (SC) linac installed in the upstream end of the old linac tunnel complete with an injector and a long transport line to bring the electron bunches to the undulator hall. The downstream third section of the old SLAC Cu linac, which had already been used to accelerate electron bunches for the LCLS project, is still to be used to provide electron bunches to the HXR undulator line in addition to the bunches coming from the SC linac. During the LCLS-II construction phase, extra funds provided fro outside of the LCLS-II project were made available to add an additional transport line to make it possible to deliver the Cu linac beam also to the SXR beamline, so that now, the beams from both the old normal conducting linac and the new superconducting linac can be used with both undulator lines. In June 2020, the first part of the project, the operation of the new beamlines with the Cu linac

Performance Measure	Threshold	Objective
Variable gap undulators	2 (soft and hard x-ray)	2 (soft and hard x-ray)
Superconducting linac-based FEL system		
Superconducting linac electron beam energy	3.5 GeV	≥ 4 GeV
Electron bunch repetition rate	93 kHz	929 kHz
Superconducting linac charge per bunch	0.02 nC	0.1 nC
Photon beam energy range	250–3,800 eV	200–5,000 eV
High repetition rate capable end stations	≥ 1	≥ 2
FEL photon quantity (10^{-3} BW)	5×10^8 (10x spontaneous @2,500 eV)	$> 10^{11}$ @ 3,800 eV
Normal conducting linac-based system		
Normal conducting linac electron beam energy	13.6 GeV	15 GeV
Electron bunch repetition rate	120 Hz	120 Hz
Normal conducting linac charge per bunch	0.1 nC	0.25 nC
Photon beam energy range	1,000–15,000 eV	1,000–25,000 eV
Low repetition rate capable end stations	≥ 2	≥ 3
FEL photon quantity (10^{-3} BW[a])	10^{10} (lasing @ 15,000 eV)	$> 10^{12}$ @ 15,000 eV

Figure 1: LCLS-II Key Performance Parameters.

beam, was ready, and commissioned during Summary and Fall of 2020. User operation on both beamlines began in late Fall of that year. This document examines how the performance of this initial part of the LCLS-II project compares with the goals as defined by the Key Performance Parameters.

Further author information: E-mail: nuhn@slac.stanford.edu

2. PERFORMANCE PREDICTIONS AND EXPECTATIONS

The **K**ey **P**erformance **P**arameters (KPPs) of the LCLS-II project are listed in a table on page 5 (figure 1) of the **G**lobal **R**equirement **D**ocument (GRD) [1]. That table is reproduced here as Fig. 1, above. It contains two data columns, labeled "Threshold" and "Objective" . The ''Threshold" column contains values that need to be met before the project can be considered completed successfully, while the values in the ''Objective" column are future, final goals.

The parameters in Fig. 1 are considered independent of each other, which means that none of them has to be achieved at the same time as any of the others in the table. For this document, only the bottom six rows of Fig. 1 are relevant and they need only to be considered for the HXR beamline. As mentioned above, operation of the SXR beamline with beams from the Cu linac is not part of the LCLS-II project and therefore not covered by these KPPs. The subject of this document is to assess how the operation of the new HXR undulator with the Cu linac compares to the KPP goals.

The expected performance of the HXR FEL, operating in SASE (**S**elf-**A**mplified **S**pontaneous **E**mission) mode with electron bunches from the Cu linac has been predicted in 2015 in the Final Design Report of the LCLS-II project. One of the figures in that document is reproduced here as Fig. 2.
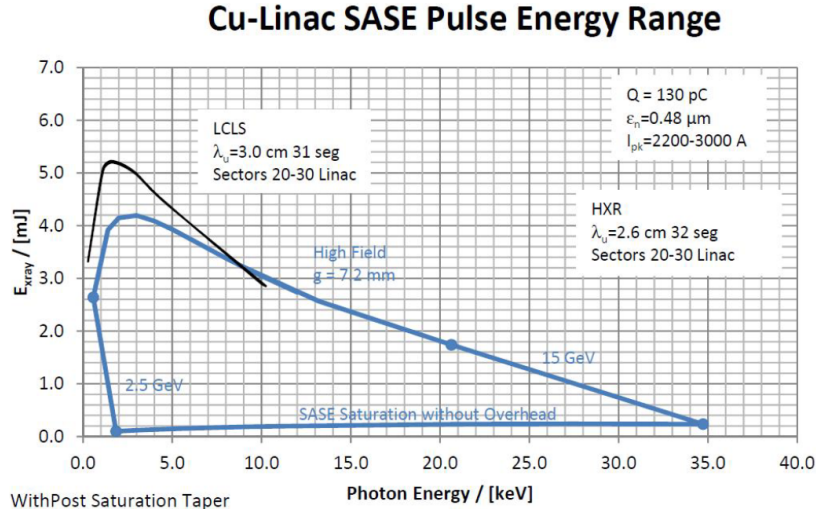

Figure 2: Performance — X-ray pulse energy vs. photon energy — predicted in 2015 for the HXR undulator line (blue) as driven by the existing Cu linac (sectors 21-30) at 120 Hz. The performance of the then existing LCLS 30-mm-period undulator line is added (black) for comparison. The new HXR undulator line was expected to deliver comparable performance at around 9 keV photon energy and was also expected to be able to provide x-rays with energies at least as high as 25 keV. (The figure is taken from the LCLS-II Final Design Report (FDR-Fig 3.11 page 3-14) [2])

The blue curve in Fig. 2 shows the limits of predicted x-ray pulse intensity ranges for the fundamental photon energies that can be generated by the HXR line with electron beams from the Cu linac. For each photon energy (except for the lowest and highest) there are two values indicated by the blue curve. The upper value represents performance at the smallest undulator gaps (highest K values), while the lower value represents performance at the largest gap at which saturation occurs before the end of the last HXR undulator segment. The blue dots in the blue curve identify sections of constant gap and constant electron energy, respectively.

As can be seen from the figure, the photon energy range of the HXR line far exceeds that of the former LCLS FEL. This comes from the smaller undulator period and smaller K values of the HXR undulator segments. (the period was reduced from $\lambda_{u,LCLS} = 30$ mm to $\lambda_{u,HXR} = 26$ mm, which reduced the maximum K value from $K_{LCLS} = 3.10$ to $K_{HXR} = 2.57$). Another consequence of that parameter change is the reduced pulse intensity at photon energies below about 9 keV that can be seen in the figure.

3. CHECKING KPP GOALS

The following sub sections compare the six KPP goals that are relevant to this document with the achieved performance values.

3.1. NORMAL CONDUCTING LINAC ELECTRON BEAM ENERGY

Electron beam energy is measured via the amount that the electron beam gets deflected in the Dogleg-2 part of the Linac-To-Undulator (LTU) part of the new beamline and in the electron beam dump (EBD). It is proportional to the current in the corresponding bending magnets when the target deflection is reached. The bending magnet current is calibrated in units of GeV and, in operations, is served by `EPICS` process variable (PV), `BEND:DMPH:400:BACT`. The highest electron beam energy used so far with the HXR beamline has been 15.3 GeV (see Tab. 1, below), which exceeds both the Threshold and Objective KPP requirements for this goal (see data row 10 in Fig. 1, above).

3.2. ELECTRON BUNCH REPETITION RATE

The electron bunch repetition rate is controlled by the timing system. The maximum rate for the Cu linac beam is 120 Hz. This was the rate that was most often used since operations began. The rate was verified by beam synchronous acquisition (BSA), which provides bunch position and charge measurements for each passing bunch with the exact time stamp for each.

This repetition rate matches both the Threshold and Objective KPP goals (see data row 11 in Fig. 1, above).

3.3. NORMAL CONDUCTING LINAC CHARGE PER BUNCH

The electron injector for the Cu linac has been delivering bunches at the Objective KPP bunch charge of 0.25 nC for most of the time during operations since the start of commissioning. These bunches are transported through linac sections L0A, L0B, L1S and L1X to BC1. At BC1, both ends of each bunch are removed to enhance FEL performance in the undulator system.

This bunch charge exceeds the Threshold KPP goal and matches the Objective KPP goal (see data row 12 in Fig. 1, above).

3.4. PHOTON BEAM ENERGY RANGE

The fundamental photon energy, E_{ph}, is proportional to the square of the electron energy, E_e

$$E_{ph} = \frac{2hc}{\lambda_u \left(1 + K^2/2\right) \left(m_e c^2\right)^2 e} E_e^2. \tag{1}$$

Eq. 1 uses the undulator period length, $\lambda_u = 26$ mm, the undulator parameter, $K \lesssim 2.57$, the electron rest energy, $m_e c^2 = 510998.95$ eV, Planck's constant, $h = 6.62607015 \times 10^{-34}$ Js, the speed of light in vacuum, $c = 299792458$ m/s and the electron's charge, $e = 1.60217663 \times 10^{-19}$ C. Tab. 1 shows two events taken from the LCLS-II archive that show the maximum and minimum photon energies generated in the HXR line. Each line in the table contains the parameters used in Eq. 1.

Table 1: Events with maximum and minimum photon energy in HXR line.

	E_{ph}	E_e	K	Event Time
max	25.252 keV	15.300 GeV	2.1844	12/12/2021 23:30:00
min	1.567 keV	4.000 GeV	2.3365	10/20/2022 19:10:00

Also of interest is the accuracy of the provided photon beam energy based on Eq. 1. Fig. 3 shows two example spectra, taken at different photon energies at the LCLS-II MFX end station, from HXR x-ray pulses accelerated by the Cu linac.

Each spectrum was fitted to obtain the central photon energy. The fitted curve is plotted in red over each measured spectrum and the central photon energy is displayed in and under each plot. These photon energies are also displayed,

together with the corresponding electron beam and undulator parameters, in Tab. 2, which shows the estimated photon energy, $E_{ph,est}$, calculated from E_e and K based on Eq. 1 and converted it into $\Delta E_e/E_e$ via

$$\frac{1}{E_{\mathrm{ph,pk}}}\left(E_{\mathrm{ph,pk,est}} - E_{\mathrm{ph,pk}}\right) = \frac{1}{E_{\mathrm{ph,pk}}}\Delta E_{\mathrm{ph,pk}} = \frac{1}{E_{\mathrm{ph,pk}}}\frac{\partial E_{\mathrm{ph,pk}}}{\partial E_{\mathrm{e}}}\Delta E_{\mathrm{e}} = \frac{1}{E_{\mathrm{ph,pk}}}\frac{2E_{\mathrm{ph,pk}}}{E_{\mathrm{e}}}\Delta E_{\mathrm{e}} = 2\frac{\Delta E_{\mathrm{e}}}{E_{\mathrm{e}}} \quad (2)$$

or

$$\frac{\Delta E_{\mathrm{e}}}{E_{\mathrm{e}}} = \frac{1}{2}\frac{\Delta E_{\mathrm{ph,pk}}}{E_{\mathrm{ph,pk}}}. \quad (3)$$
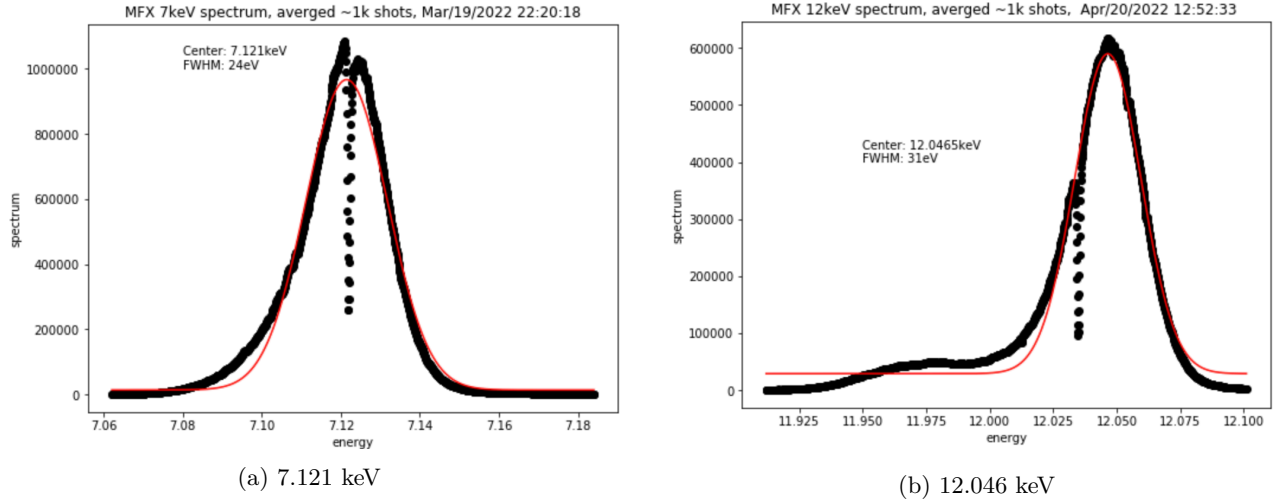

(a) 7.121 keV

(b) 12.046 keV

Figure 3: LCLS-II MFX spectra taken with x-ray pulses based on electron bunches accelerated by the Cu linac. [provided by Sanghoon Song, SLAC, private communication]

The photon energies obtained from the spectra are about 0.4 % larger than expected from the estimates based on electron beam energy measurements. That difference is consistent with the assumption that the actual electron energy at the first undulator segment is 0.2% larger than the value extracted from the dump bend current (see SubSection 3.1), which can be considered an excellent agreement.

Table 2: Events with maximum and minimum photon energy in the HXR beamline since the start of commissioning.

Acquisition Date	4/20/2022 12:52:33	3/19/2022 22:10:18	
Central Photon Energy, $E_{\mathrm{ph,pk}}$	12.0465	7.121	keV
Photon Bandwidth, $\Delta E_{\mathrm{ph,FWHM}}$	31	24	eV
Electron Energy, E_{e}	11.818	9.026	GeV
Undulator, K	2.5501	2.5284	
Charge, Q	193	201	pC
Peak Current, I_{pk}	3627	2099	A
Pulse Intensity, E_{xray}	1.6	2.1	mJ
Estimated Photon Energy, $E_{\mathrm{ph,pk,est}}$	11.999	7.091	keV
Photon Energy Difference, $\Delta E_{\mathrm{ph,pk}}$	-47.9	-30.1	eV
$\Delta E_{\mathrm{ph,pk}}/E_{\mathrm{ph,pk}}$	-0.40%	-0.42%	
$\Delta E_{\mathrm{e}}/E_{\mathrm{e}}$	-0.20%	-0.21%	

The maximum achieved photon energy shown in Tab. 1 exceeds both the Threshold and the Objective KPP goals (see data row 13 in Fig. 1, above), while the minimum achieved photon energy shown in Tab. 1 does not go quite as low as either the Threshold or the Objective KPP goals (1 keV), but comes quite close. The treatment in this subsection should make it clear that the minimum KPP photon energies can be reached by just reducing the electron energy by a small amount, well within the available energy range. This has not yet been tried because, so far, there was no user request for these energies.

3.5. LOW REPETITION RATE CAPABLE END STATIONS

The following Low Repetition Rate Capable End Stations are in operation at 120 Hz pulse repetition rate in the HXR beamline:

1. **CXI** - The **C**oherent **X**-ray **I**maging instrument makes use of the unique brilliant hard X-ray pulses to perform a wide variety of experiments utilizing various techniques.

2. **MEC** - The particular strength of the **M**atter in **E**xtreme **C**onditions instrument is to combine the unique LCLS beam with high power optical laser beams, and a suite of dedicated diagnostics tailored for this field of science.

3. **MFX** - The **M**acromolecular **F**emtosecond Crystallography instrument primarily makes use of the ability for short pulses of **X**-rays to limit damage to samples during the exposure.

4. **XCS** - The unprecedented brilliance and narrow pulse duration of the x-ray pulses provides a unique opportunity to observe dynamical changes of large groups of atoms in condensed matter systems over a wide range of time scales using **C**oherent **X**-ray **S**cattering in general and X-ray Photon Correlation Spectroscopy (XPCS) in particular.

5. **XPP** - The **X**-ray **P**ump-**P**robe instrument predominantly uses ultra-short optical laser pulses to generate transient states of matter which are subsequently probed by the hard X-ray pulses.

The number of end stations capable of operation at low repetition rate exceeds the Threshold and the Objective KPPs (see data row 14 in Fig. 1, above).

3.6. FEL PHOTON QUANTITY

The FEL photon quantity or the number of FEL photons per x-ray pulse can be calculated from the total FEL energy in the x-ray pulse.

3.6.1. X-Ray Pulse Intensity Measurements

The total FEL energy contained in the x-ray pulse is estimated by measuring the loss of the kinetic energy of the electrons, i.e, by measuring the changes of the average vertical position of the bunch electrons in the dump line (when turning off the FEL interaction) after the vertical bend magnets, where the momentum dispersion is large. This method, called 'eloss scan', was developed in 2009 during commissioning of the original LCLS undulator line and is described in the First Lasing paper [3].

Fig. 4 represents an example of an eloss scan. The FEL interaction is controlled by a horizontal corrector just upstream of the entrance to the undulator hall. Its amplitude is plotted on the x axis. The y axis shows the energy loss calculated from the vertical position of the electron bunches in the dump line. As can be seen in the figure, there is a corrector strength (x axis; about 9.3 kGm in this particular arrangement) for which the FEL energy loss (y axis) is largest. At this point, the corrector amplitude is just right for launching the electron bunch onto a straight trajectory through the undulator line. Any deviation from that corrector amplitude, positive or negative, will cause the electrons to oscillate (execute betatron oscillations) relative to the originally straight trajectory. Those oscillations reduce the FEL process and thus the FEL energy loss. As can be seen from the figure, for large deviations of the corrector strength, the FEL energy loss becomes smaller than energy losses from other effects (synchrotron radiation and wakefields), which are independent of trajectory errors and form a baseline in the plot. The maximum increase of energy loss per electron above that baseline multiplied by the electron bunch charge yields the total energy lost to the FEL process which is the source of the energy of the x-ray pulse.
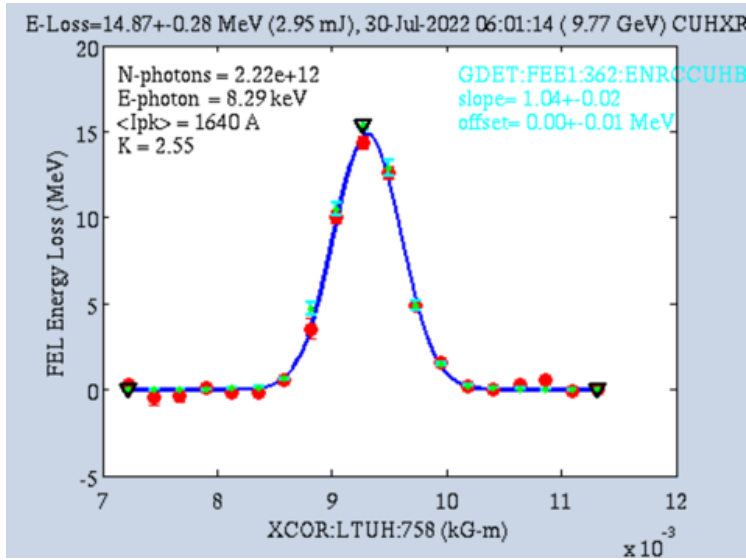
Figure 4: The figure shows how changing the strength of a horizontal corrector just before the entrance to the undulator hall (XCOR:LTUH:758), affects the average energy loss of the bunch electrons (eloss scan). The scan is used for the measurement of the FEL x-ray pulse energy.

This method is routinely used to measure FEL x-ray pulse energies (with 5% rms precision) throughout the entire operational wavelength range. This electron-based x-ray energy measurement is also used to calibrate the gas detectors, which measure the relative x-ray pulse energy in each pulse. The particular scan performed on 7/30/2022 6:01:14 and shown in Fig. 4 resulted in an x-ray energy per pulse of 2.85 mJ.
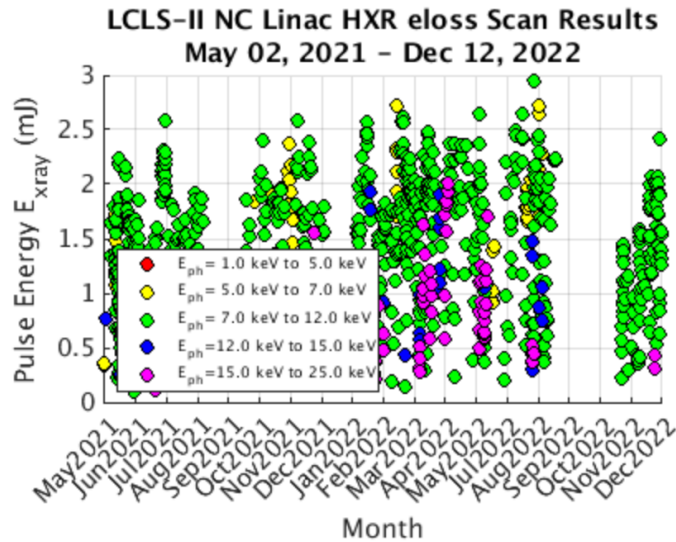

Figure 5: Results of eloss scans performed by the operators on the HXR bunches between 5/1/2021 and 12/12/2022.

Fig. 5 is a plot of the results of all eloss scans with acceptable fit outcome performed by the accelerator operators during the period indicated on top of the plot. The color code, which is explained in the legend included in the figure, indicates the photon energy range in which the FEL operated during each eloss scan.

Fig. 6, an alternate view of the data points in Fig. 5, is a plot of eloss scan results vs. photon energy. Here, the color code indicates the peak current at which the FEL operated during each scan. It demonstrates how operations at higher photon energy requires higher peak currents. The maximum expected amplitudes have been predicted in the FDR (see Fig. 2). The upper blue line in that figure, which corresponds to performance predictions when operating
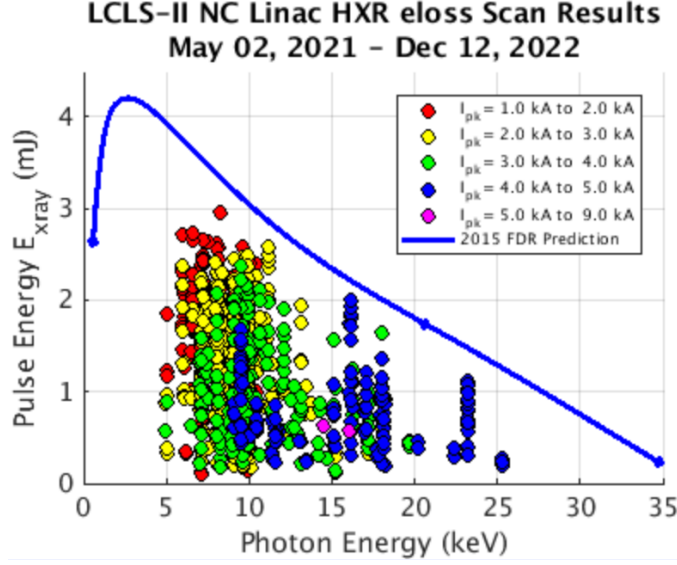
Figure 6: Results of eloss scans performed by the operators on the HXR bunches between 5/1/2021 and 12/12/2022 plotted against the corresponding photon energy. Also added to the plot is the performance prediction from Fig. 2

the undulator segments at their smallest gap or largest K values, has been copied into Fig. 6. Fig. 6 shows that for a given photon energy, for which beam delivery took place, the eloss scan results cover almost the entire pulse energy (intensity) range from very low to close to the predicted maximum. This is a demonstration of the sensitivity of the optimum FEL performance to gun, linac and transport line parameters. Tuning these parameters to reach the optimum can take many days. It is also quite extraordinary that the achieved optima seem to approach the predicted values quite closely.

3.6.2. Photons per Pulse

Fig. 7 shows the data from Fig. 6 with the vertical axis converted from x-ray pulse energy, E_{xray}, to x-ray pulse photon number, N_{ph}, via the corresponding photon energy, E_{ph}. The conversion is done via

$$N_{\mathrm{ph}} = \frac{E_{\mathrm{xray}}}{E_{\mathrm{ph}}}. \tag{4}$$

The Objective KPP goal for the photon number specifies $> 10^{12}$ photon within 0.1% bandwidth (Fig. 1). The conversion from the total photon number per pulse, N_{ph}, to the photon number per pulse within a relative bandwidth of 10^{-3}, i.e. within a range of photon energies of $E_{\mathrm{ph}} \times 10^{-3}$, $N_{\mathrm{ph,0.1\%BW}}$, is given by

$$N_{\mathrm{ph,0.1\%BW}} = 10^{-3} N_{\mathrm{ph}} \frac{\sqrt{8\log(2)}}{\sqrt{2\pi}} \frac{E_{\mathrm{ph}}}{\Delta E_{\mathrm{ph,FWHM}}} \approx 0.9394 \times 10^{-3} N_{\mathrm{ph}} \frac{E_{\mathrm{ph}}}{\Delta E_{\mathrm{ph,FWHM}}} \tag{5}$$

The position of the red star in Fig. 7, calculated as

$$N_{ph} = N_{\mathrm{ph,0.1\%BW}} \frac{\Delta E_{\mathrm{ph,FWHM}}}{0.9394 \times 10^{-3} E_{\mathrm{ph}}} = 2.48 \times 10^{12}, \tag{6}$$

represents the Objective KPP goal from data row 15 (last data row) in Fig. 1, in terms of the total number of FEL photons per pulse, with $N_{\mathrm{ph,0.1\%BW}} = 10^{12}$ photons, $E_{\mathrm{ph}} = 15$ keV and $\Delta E_{\mathrm{ph,FWHM}} = 35$ eV, the latter extrapolated from Tab. 2 under the assumption of a slight peak current increase, as normally used towards the higher electron beam energies. This KPP goal (marked with a red star in Fig. 7) exceeds the predicted maximum photon number ($N_{ph} = 0.96 \times 10^{12}$, corresponding to $N_{\mathrm{ph,0.1\%BW}} = 0.39 \times 10^{12}$), based on current and previous electron beam parameters, which is marked with a green star in Fig. 7 at the 15-keV photon energy, and was therefore not a
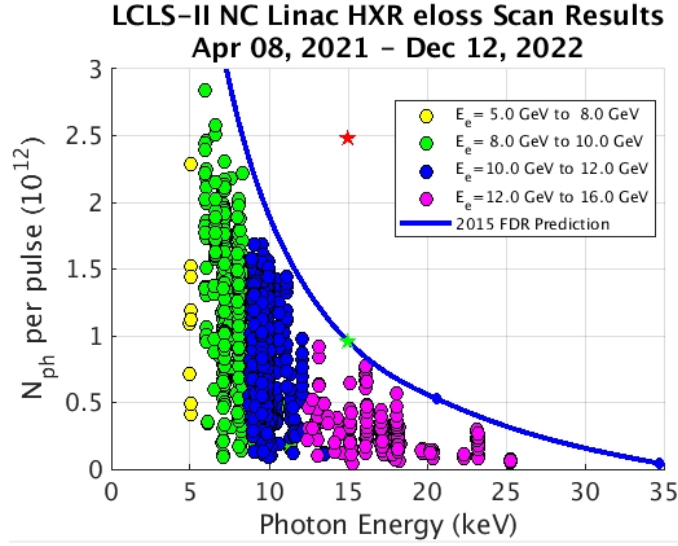
Figure 7: Results of eloss scans (in terms of photon number per x-ray puse) performed by the operators on the HXR bunches between 5/1/2021 and 12/12/2022 plotted against the corresponding photon energy. Also added to the plot is the performance prediction from Fig. 2 converted from E_{xray} to photon number per pulse, N_{ph}
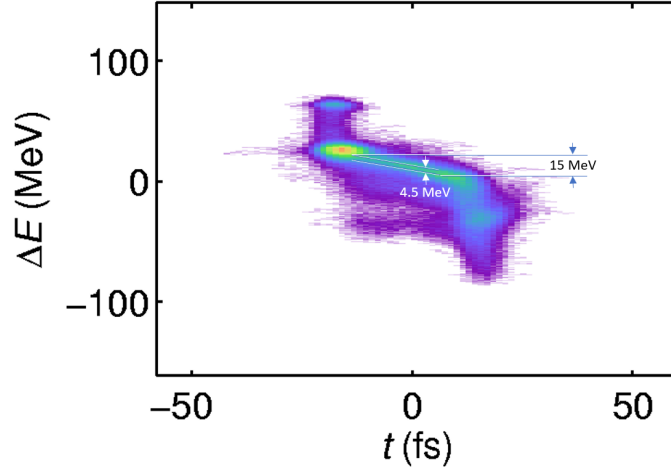

Figure 8: LCLS-II Cu Linac electron beam phase space at the end of the undulator line measured by the transverse cavity system (XTCAV) on April 20, 2022 at 16:36. The lines added to the plot indicate the phase space range of the electrons participating in the FEL process at saturation. The vertical separation of the sloped lines is due to the FEL process (stable buckets), while the slope is due to the initial energy chirp introduced during bunch compression in the linac. The purple bar at the bottom of the image shows the electrons left in the buckets after post-saturation tapering.

consistent value to be used for this goal. It is conceivable, though, that with future improvements to the injector-accelerator-transport complex, better electron beam parameter (especially emittance) can be achieved such that this Objective KPP goal could be achieved.

The origin of the amount of $\Delta E_{\mathrm{ph,FWHM}}$, listed in Tab. 2, is dominated by the bunch energy chirp introduced in the linac bunch compressors. Fig. 8 shows an electron beam phase space image measured a few hours after the spectrum in Fig. 3b was recorded. The additional lines added to the figure show the source of the spectral width of the corresponding x-ray pulse. The 15 MeV energy width of the electron bunch corresponds to the 31 eV width of the spectrum in the table. This phase space distribution is typical, although further chirp suppression is possible, which could improve the number of x-ray photons within the requested bandwidth.

Fig. 7 shows, that, even though the total number of photons reached is 0.6×10^{12} at exactly 15 keV, corresponding to $N_{\text{ph,0.1\%BW}} = 0.24 \times 10^{12}$, the maximum x-ray pulse photon numbers at photon energy values above and below the specific KPP photon energy of 15 keV have come quite close to their expected maximum values. More future tuning time might improve this result. More user experiments at 15 GeV would help.

4. SUMMARY

The LCLS-II project has completed commissioning the new HXR undulator line with electron bunches accelerated by the normal-conducting Cu linac. Tab. 3 compares the achieved performance values to the KPP goals.

Table 3: Summary comparison of KPP goal vs. achieved values.

Peformance Measure	Threshold		Objective		Actual	Units
Normal conducting linac based beam energy	13.6	✓	15.0	✓	15.3	GeV
Electron bunch repetition rate	120	✓	120	✓	120	Hz
Normal conducting linac charge per bunch	0.1	✓	0.25	✓	0.25	nC
Photon beam energy range	$1.0 - 15.0$	(✓)	$1.0 - 25.0$	(✓)	$1.6 - 25.3$	keV
Low repetition rate capable end stations	≥ 2	✓	≥ 3	✓	5	
FEL photon quantity (10^{-3} BW@15,000 eV)	10^{10} (lasing)	✓	$> 10^{12}$		0.24×10^{12}	ph/pulse

These goals, both Threshold and Objective, have been met in all but three cases (see check marks in Tab. 3) and have been exceeded in some cases. The three exception are

- (1,2) The lower goal of the photon energy range of 1 keV has not yet been met for either the Threshold or the Objective goals (see check marks in parenthesis) because no attempt was made to run at 1 keV. The lowest photon energy attempted so far was 1.6 keV. To produce 1-keV photons, a 3.4-GeV electron beam needs to be sent through the HXR undulator line while the undulator K values are set close to the maximum (around 2.55). This is expected to be just a formality and a matter of beam time scheduling.

- (3) The Objective goal to produce x-ray pulses with 10^{12} photons in a 0.1% bandwidth range at a photon energy of 15 keV, has not yet been reached. This goal will need further improvements to electron beam parameters (especially emittance) to reach this goal.

The bottom line is that all KPP parameters required for successfully completing the project (Threshold) have for all intents and purposes been met for operation of the new undulator lines with the beam from the Cu linac.

References

[1] J. Galayda, "Linac Coherent Light Source II Project Requirements Document," 2 December 2015. LCLSII-1.1-GR-0018-R1.

[2] LCLS-II Project Team, "Linac Coherent Light Source II (LCLS-II) Project Final Design Report," 22 November 2015. LCLSII-1.1-DR-0251-R0.

[3] P. Emma, R. Akre, J. Arthur, R. Bionta, C. Bostedt, J. Bozek, A. Brachmann, P. Bucksbaum, R. Coffee, F.-J. Decker, Y. Ding, D. Dowell, S. Edstrom, A. Fisher, J. Frisch, S. Gilevich, J. Hastings, G. Hays, Ph. Hering, Z. Huang, R. Iverson, H. Loos, M. Messerschmidt, A. Miahnahri, S. Moeller, H.-D. Nuhn, G. Pile, D. Ratner, J. Rzepiela, D. Schultz, T. Smith, P. Stefan, H. Tompkins, J. Turner, J. Welch, W. White, J. Wu, G. Yocky, and J. Galayda, "First Lasing and Operation of an Å ngstrom-Wavelength Free-Electron Laser," *nature photonics* **4**, p. 644, 2010.